

NUMERICAL AND EXPERIMENTAL PRESSURE DISTRIBUTIONS OVER A SOUNDING VEHICLE MODEL

Guilherme Bertoldo, gbertoldo@utfpr.edu.br

Universidade Tecnológica Federal do Paraná (UTFPR),
CEP 85601-970, Francisco Beltrão-PR, Brazil.

Ana Cristina Avelar, anacristina.avelar@gmail.com

João Batista Falcão Filho, jb.falcao@ig.br

Jéssica Jia Ling Hsu, jessicajl.hsu@hotmail.com

Instituto de Aeronáutica e Espaço (IAE),
CEP 12228-904, Pça. Marechal Eduardo Gomes, 50, São José dos Campos, São Paulo, Brazil

Carlos Henrique Marchi, marchi@ufpr.br

Federal University of Paraná (UFPR)
Curitiba, PR, Brazil

***Abstract.** The surface pressure distribution over a model of the Brazilian VS-40 sounding vehicle was measured in a transonic wind tunnel and numerically determined for four values of free-stream Mach numbers: 0.4, 0.6, 0.8 and 1.0. The experimental data were obtained through the traditional technique of pressure taps, while the numerical solution was obtained by solving the Euler equations based on a finite volume approach. Despite the simplified model for the flow simulation, a reasonable agreement between theoretical and experimental data was observed. The highest relative difference between experimental and numerical results was of 7.0% for pressure.*

***Keywords:** Surface Pressure, CFD, Validation, Transonic wind tunnel, Pressure taps*

1. INTRODUCTION

Quantitative determination of surface pressure over flight vehicles is very important for understanding their aerodynamic performance (Liu and Sullivan, 2005). This determination may be done either experimentally, using wind tunnels, for instance, or theoretically, using Computational Fluid Dynamics (CFD) software. These approaches, however, are not independent. The validation of the solutions obtained from CFD depends on experimental data. On the other hand, experimentation planning and interpretation of results may be improved through the flow prediction from reliable software.

This work, which resulted from a cooperation between the CFD group of the Federal University of Paraná (UFPR) and experimentalists of the Institute of Aeronautics and Space (IAE), deals with the numerical and experimental determination of the surface pressure distribution over a model of the Brazilian sounding vehicle VS-40 caused by air flow under the free-stream Mach numbers 0.4, 0.6, 0.8 and 1.0 for zero angle of attack.

The pressure measurements were performed using tap holes of 0.5 mm diameter on specific positions over a preliminary version of the VS-40 model in the transonic wind tunnel located in the IAE, while the numerical results were obtained by solving the Euler equations based on a finite volume method.

In the following sections, both the numerical and experimental methodologies are briefly described and the experimental and numerical pressure distribution over nine points along the VS-40 model are presented in tables with their experimental uncertainty and estimated numerical error, respectively. The results of both methodologies are compared and some conclusions are drawn.

2. METHODOLOGY

2.1 Description of the experiments

Surface pressure measurements were conducted in the Pilot Transonic Wind Tunnel (Tunel Transônico Piloto - TTP) located at Aerodynamics Division (ALA) of the Institute of Aeronautics and Space (IAE). Figure 1 shows a frontal view of the facility with the plenum chamber open. The facility has a conventional closed circuit, continuously driven by a main compressor of 830 kW of power, and additionally an intermittent injection system which operates in a combined mode, for at least 30 seconds. Its test section is 30 cm wide, 25 cm high and 80 cm length, with slotted walls. TTP has automatic pressure controls from 0.5 bar to 1.25 bar, with Mach number varying between 0.2 and 1.3 as well as control of temperature and humidity in its test section. A detailed description of TTP wind tunnel can be found in Falcão Filho and Mello (2002), and a historical description of the tunnel is presented in Falcão Filho et al. (2009).



Figure 1. TTP wind tunnel frontal view.

TTP is a facility very appropriate for conducting tests with basic geometry vehicles, quantitative tests of airplane simplified models, tests in developing of new aerodynamic transonic profiles and to perform basic and academic researches.

In the present work it was used the most traditional method for surface pressure measurements, the technique of pressure taps. This method consists of installing arrays of small orifices on a model surface and connecting them through small flexible tubes to pressure transducers. This technique, relatively simple, provides good results, but has also some drawbacks. It can be costly in price and time to manufacture and to prepare a model with the hundreds of pressure taps necessary to provide a reasonable resolution, mainly when one is dealing with industrial tests using big models. However, in spite of the disadvantages, this technique has a very high reliability. The measurements errors are in general not bigger than $\pm 0.03\%$ or ± 20 Pa using pressure scanner of ± 10 psi from Esterline, model ESP-32HD. In the present work, tap holes of 0.5 mm diameter were installed on a 1:34 scale model of the sounding vehicle VS-40, and pressure sensors located outside of the plenum chamber supply the pressure readings. According to SAE report, the hole dimension causes a 0.2% static pressure reading error, which is relatively high comparing to the pressure sensor error. As shown in Fig. 2, a hole diameter of 0.2 mm yields an error of 0.03% and it can be noticed from this picture that the smallest the hole, the smallest the error. This explains the difficulty and onerousness of building this kind of model (SAE, 1990).

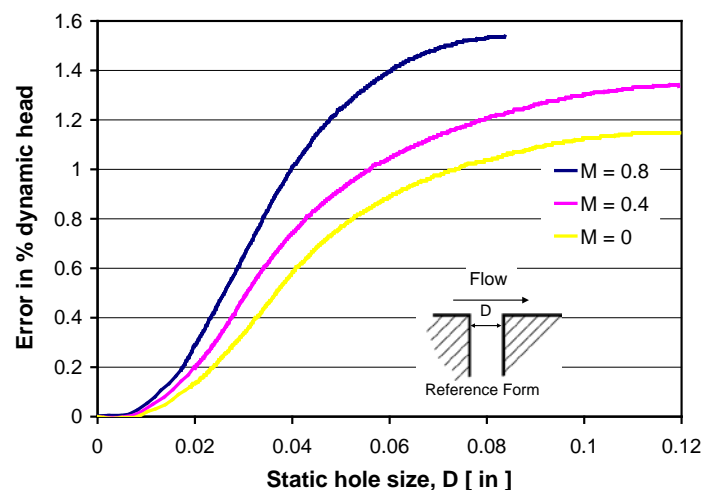


Figure 2. Effect of taps holes size and Mach number on wall static tap pressure reading (SAE, 1990).

In this study just the fore-body region of the model, Fig. 3a, was investigated for free-stream Mach number values of 0.4, 0.6, 0.8 and 1.0. In Fig. 3a it is shown also the positions of pressure holes and Fig. 3b presents a picture of the VS-40 model used in present study. The fore-body of the model is composed by a hemisphere-cone followed by a cylinder, as depicted in Fig. 4, where $l_o = 42.68$ mm, $r_c = 14.95$ mm, $r_d = 0.6$ mm, $\alpha = 11^\circ$ and $\theta = 11^\circ$. As can be

seen, there is a small difference between the nose cone base radius and the cylinder radius, resulting in a backward step. The reason is that this model was fabricated in 2009 and the rocket nose is a preliminary version of the Sub-orbital SARA, a Brazilian platform for microgravity experiments.

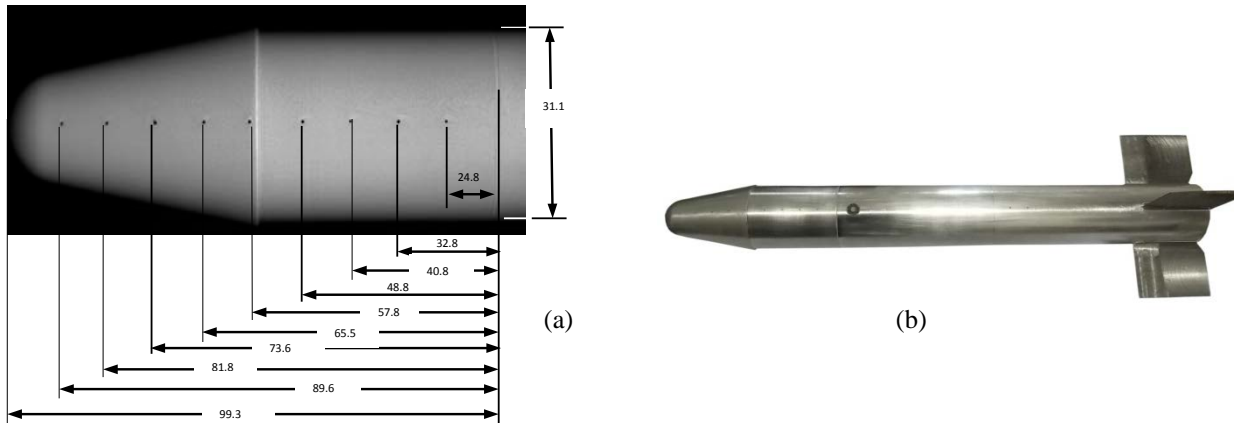


Figure 3. VS-40 model: (a) fore-body region and (b) model installed in TTP test section.

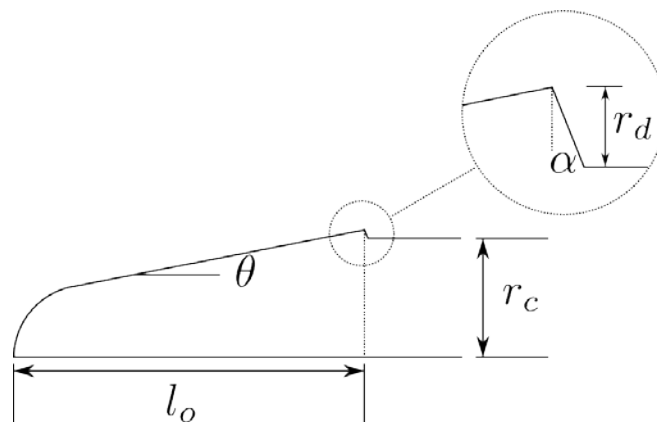


Figure 4. Geometric configuration of the model fore-body.

2.2 Description of the simulations

In this work, the flow is modeled by the time dependent and compressible Euler equations. In an axisymmetric flow these equations are written as:

Mass conservation equation

$$\frac{\partial \rho}{\partial t} + \frac{\partial(\rho u)}{\partial x} + \frac{1}{y} \frac{\partial(\rho y v)}{\partial y} = 0 \quad (1)$$

Momentum conservation equation – axial component

$$\frac{\partial(\rho u)}{\partial t} + \frac{\partial(\rho u u)}{\partial x} + \frac{1}{y} \frac{\partial(\rho y u v)}{\partial y} = -\frac{\partial p}{\partial x} \quad (2)$$

Momentum conservation equation – radial component

$$\frac{\partial(\rho v)}{\partial t} + \frac{\partial(\rho uv)}{\partial x} + \frac{1}{y} \frac{\partial(\rho y v v)}{\partial y} = -\frac{\partial p}{\partial y} \quad (3)$$

Thermal energy conservation equation

$$\frac{\partial(\rho T)}{\partial t} + \frac{\partial(\rho u T)}{\partial x} + \frac{1}{y} \frac{\partial(\rho y v T)}{\partial y} = \frac{1}{c_p} \left[\frac{\partial p}{\partial t} + u \frac{\partial p}{\partial x} + v \frac{\partial p}{\partial y} \right] \quad (4)$$

In Eqs. (1)-(4), t is the time, x and y are, respectively, the axial and radial coordinates (see Fig. 5), ρ , p , T and c_p are, respectively, the gas density, pressure, temperature and specific heat at constant pressure, and u and v are the axial and radial components of the gas velocity.

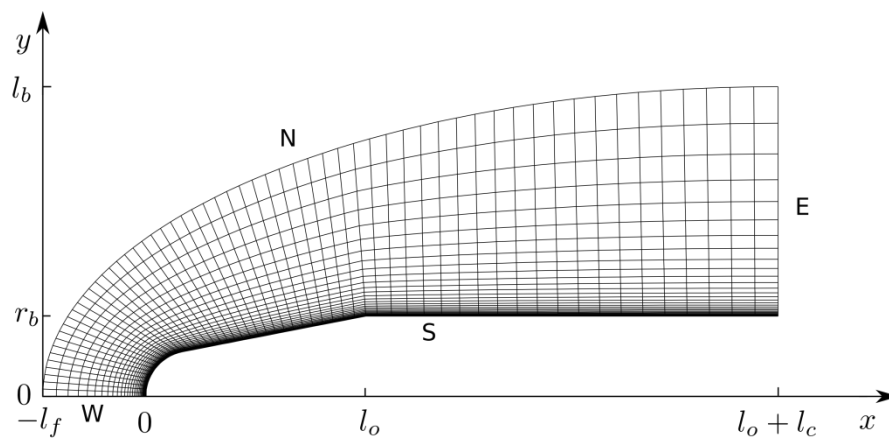


Figure 5. Illustration of the domain of calculation and its discretization.

The state equation of the ideal gases,

$$p = \rho RT \quad (5)$$

is the closure relation to Eqs. (1)-(4). In Eq. (5), R is the gas constant.

The set of Eqs. (1)-(5) were solved numerically by the Mach2D algorithm, which is under development by the CFD group at UFPR. This algorithm is based on the finite volume method using structured grid, collocated formulation and curvilinear coordinates. It uses first order accurate approximations for the advective terms and second order accurate for diffusive ones. In this paper, the stationary solution is obtained by solving the time dependent Euler equations following a false transient to accelerate the convergence. The details about the discretization of the differential equations can be found in Araki (2009). The air is assumed to be a mixture of Ar, O₂ e N₂ with molar fractions of 1%, 21% e 78%, respectively. The thermophysical properties are constant (equal to their free-stream values) and calculated for each molecular specie according to the formulas of McBride et al. (1993) and for the mixture according to Sutton and Biblarz (2001) and Bird et al. (2002).

The domain of calculation, simplified due to the axial symmetry, is show schematically in Fig. 5. The south boundary (S) represents the body surface, a hemisphere-cone followed by a cylinder. Indeed, this is an approximation to the real geometry, which has a small step in the cone-cylinder matching point, previously mentioned. The north boundary (N) is a semi-ellipse. The grid is generated by the algebraic method in such a way that the volumes are concentrated near the body surface and near the stagnation point. The x coordinate of the north boundary is discretized using a power-law distribution with exponent equals 2. The same distribution is applied to the x coordinate of the south boundary, except that, along the nose cone, the exponent is set to 2, while along the cylinder, the exponent is adjusted in such a way that the width of the volumes contiguous to the cone-cylinder matching point is the same. The segment of lines connecting the north and south boundaries are discretized in such a way that the distance between two successive

points form a geometric progression. The smallest distance occurs in the neighborhood of the south boundary and is defined as a multiple c_{bl} of the estimated width of the boundary layer δ in the case of a viscous flow:

$$\delta = \sqrt{\frac{\mu_{\infty}(l_o + l_c)}{\rho_{\infty}u_{\infty}}}, \quad (6)$$

where μ_{∞} , ρ_{∞} and u_{∞} are, respectively, the free-stream viscosity, density and speed. In spite of the flow not be viscous, viscosity is considered only to calculate a reference length (δ). The values of c_{bl} are presented in the next section.

Over the south boundary, the slip boundary condition is applied to the velocity field and the null normal gradient is applied to the pressure and to the temperature. Over the north boundary (N), the flow is undisturbed and its properties are prescribed. The west boundary (W) is the symmetry line, so the symmetry boundary conditions are applied. Finally, in the east boundary (E), the parabolic boundary condition models the outflow.

3. RESULTS

The pressure measurements were performed based on the stagnation temperature T_0 and pressure p_0 of Tab. 1 for the four nominal values of the free-stream Mach number: 0.4, 0.6, 0.8 and 1.0. This table also shows the measured values of the Mach number. The values in parenthesis indicate the experimental uncertainty, *i.e.*, 0.4007(8) means 0.4007 ± 0.0008 . The pressure distribution data over nine points along the model surface are presented in Tab. 2.

Table 1. Mach numbers and stagnation temperature and pressure.

M	M (real)	T_0 (K)	p_0 (kPa)
0.4	0.4007(8)	306.6(8)	93.70(12)
0.6	0.6000(6)	306.35(8)	93.702(78)
0.8	0.7996(6)	311.1(5)	93.710(84)
1.0	0.9977(9)	313.9(3)	93.701(86)

Table 2. Experimental pressure distribution over the surface of the VS-40 model.

x (m)	p (kPa)			
	$M = 0.4$	$M = 0.6$	$M = 0.8$	$M = 1.0$
0.0097	82.830(94)	70.141(98)	60.90(37)	37.83(16)
0.0175	84.155(94)	74.474(76)	63.599(65)	56.614(53)
0.0257	83.887(95)	73.645(76)	62.436(64)	54.789(58)
0.0338	83.280(94)	72.403(76)	60.808(64)	53.747(56)
0.0415	80.915(91)	67.548(74)	53.608(90)	48.177(46)
0.0505	83.486(94)	71.484(78)	52.953(62)	37.220(62)
0.0585	83.663(94)	73.226(78)	60.690(68)	40.798(67)
0.0665	83.712(95)	73.273(78)	61.850(66)	43.000(82)
0.0745	83.759(94)	73.336(78)	61.772(65)	44.15(12)

In order to perform the numerical calculations, the free-stream pressure and temperature were calculated from the free-stream Mach number and stagnation pressure and temperature of Tab. 1 assuming a specific heat ratio of $\gamma = 1.4$ (Anderson, 2003). The geometric parameters l_f , l_b and l_c of Fig. 5 were set to 32 m, 32 m and 0.8 m, respectively, except for $M = 0.4$, for which l_f and l_b were set to 40 m. Beside these parameters, c_{bl} was set to 0.5. In order to evaluate the influence of the geometric parameters on the pressure over the south boundary (more precisely, on the points where the pressure was measured), some tests were carried out. In the first test, the values of l_f , l_b were halved, while l_c , as well as, c_{bl} were kept constant. In the second test, l_f , l_b and c_{bl} were kept constant, while l_c was halved. It was found out that this choice of parameters does not affect the pressure over the south boundary up to 0.07%, 0.2%, 0.6% and 2.7% for $M = 0.4, 0.6, 0.8$ and 1.0. In the third test, c_{bl} was doubled, while l_f , l_b and l_c were held constant. The maximum effect of c_{bl} over the surface pressure was of 0.05%, 0.08%, 0.12% and 1.6% for $M = 0.4, 0.6, 0.8$ and 1.0, respectively. All tests were performed on a grid of 480 x 240 volumes (480 along the axial direction and 240 along

the radial direction). Finally, the geometric parameters l_f , l_b , l_c and c_{bl} were held constant and the number of volumes in the grid were doubled, in order to estimate the discretization error. This error was estimated using the Grid Convergence Index (GCI) (Roache, 2009). According to this estimator, given two numerical solutions, *e.g.*, φ_1 and φ_2 , obtained in grids with partitions h_1 and h_2 , the estimated discretization error U_{GCI} of φ_1 is given by

$$U_{GCI} = F_s \frac{|\varphi_1 - \varphi_2|}{r^{p_L} - 1}, \quad (7)$$

where $F_s = 3$ is the safety factor, $r = \frac{h_2}{h_1} = 2$ is the refinement ratio and $p_L = 1$ is the theoretical order of accuracy of the discretized equations.

The pressure distributions obtained numerically in grids of 960 x 480 volumes and their estimated error are shown in Tab. 3.

Table 3. Numerical pressure distribution over the surface of the VS-40 model.

x (m)	p (kPa)			
	$M = 0.4$	$M = 0.6$	$M = 0.8$	$M = 1.0$
0.0097	83.46428(89)	72.626(17)	60.63(19)	35.5(85)
0.0175	84.038(33)	73.843(77)	62.483(95)	54.7(24)
0.0257	83.843(52)	73.45(13)	61.89(17)	53.4(16)
0.0338	83.273(96)	72.26(24)	60.10(29)	51.7(21)
0.0415	80.91(59)	67.3(15)	52.4(17)	45.0(49)
0.0505	82.68(11)	70.89(41)	56.7(29)	34.8(59)
0.0585	83.220(50)	72.07(14)	59.3(10)	39.6(62)
0.0665	83.445(29)	72.550(78)	60.07(32)	43.0(47)
0.0745	83.567(19)	72.805(48)	60.48(14)	45.3(30)

In order to help understanding the comparison between experimental and numerical results, both data were plotted together in Fig. 6 with their estimated uncertainty/error. The greatest absolute value of the relative difference between the results were of 0.97%, 3.5%, 7.0% and 6.6% for $M = 0.4$, 0.6, 0.8 and 1.0, respectively. These results seem reasonable, taking into account the simplified geometry applied in the simulation, the first order approximation of the numerical calculations and the simplified fluid dynamics model, which does not include dissipative effects. Despite of that, improvements in the software are still necessary in order to obtain more reliable predictions.

4. CONCLUSIONS

The pressure distribution over a model of the VS-40 was determined experimentally and numerically for subsonic and transonic flow at zero angle of attack. Taking into account the simplified model for the flow simulation and the first order of accuracy of the numerical approximations, comparisons show a reasonable agreement between the two approaches. The greatest absolute value of the relative difference between experimental and numerical results was of 7.0% for pressure. In further studies, special attention must be paid to the order of accuracy of the numerical approximations. While first order approximations are sometimes necessary when dealing with shock waves or non-smooth geometries (as in the present work), higher order approximations are desirable. Another point that must be addressed is the implementation of artificial boundary conditions, in order to reduce the computational domain and, consequently, the computational effort. Verification and validation of the results of the simulations, will allow one to improve the mathematical model used in the Mach2D algorithm. As the algorithm becomes more reliable, their results will be used for planning new experiments or even for flow predictions under conditions where the experiments cannot be carried out.

5. ACKNOWLEDGMENTS

The authors thank CNPq (Conselho Nacional de Desenvolvimento Científico e Tecnológico, Brazil) and CAPES (Coordenação de Aperfeiçoamento de Pessoal de Nível Superior, Brazil) for their financial support. The last author is supported by a CNPq scholarship.

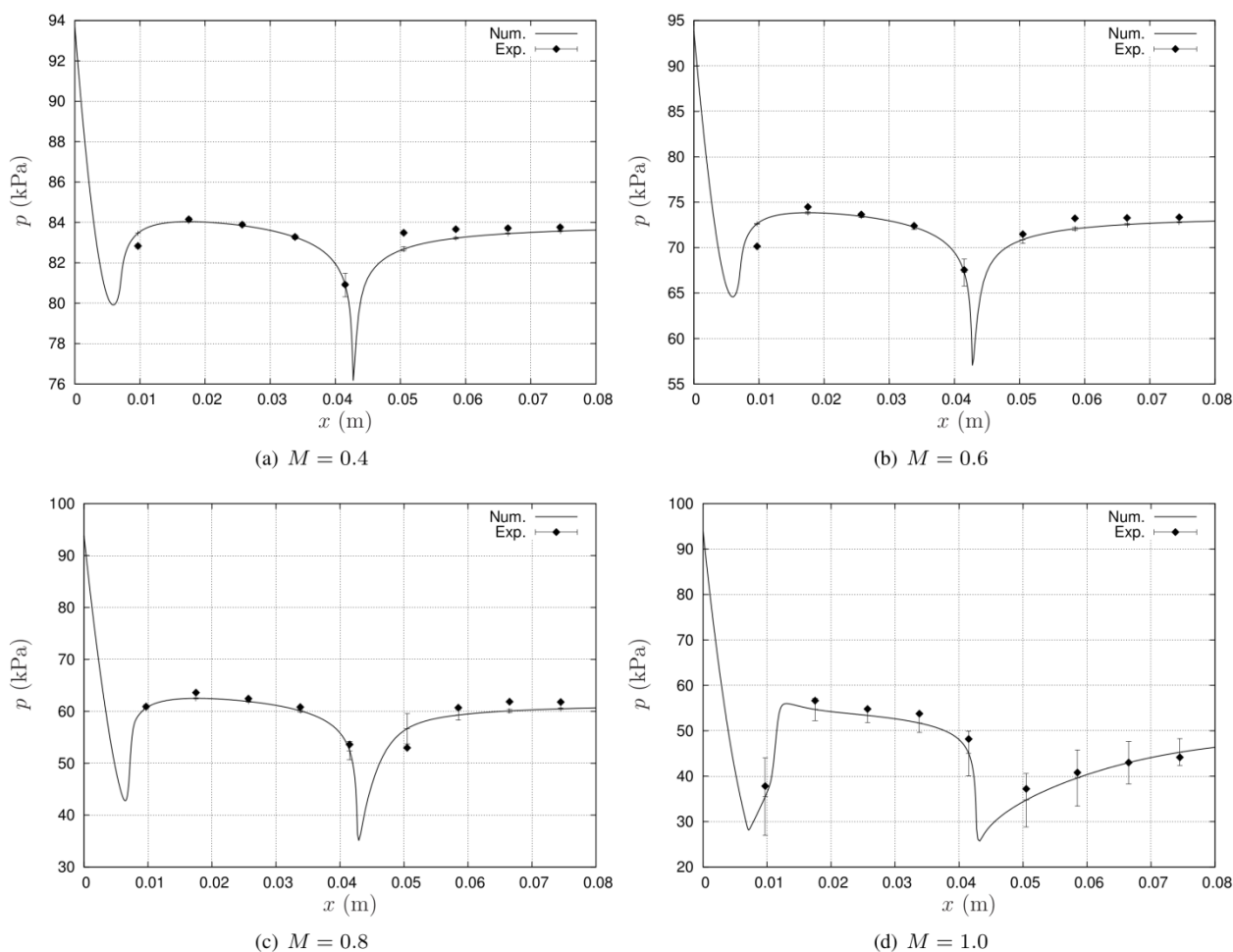


Figure 6. Numerical and experimental pressure distribution for (a) $M = 0.4$, (b) $M = 0.6$, (c) $M = 0.8$ and (d) $M = 1.0$.

6. REFERENCES

- Anderson, Jr., J.D., 2003. Modern compressible flow: with historical perspective. McGraw-Hill, New York, 3rd edition.
- Araki, L.K., 2007. Verificação de soluções numéricas de escoamentos reativos em motores-foguete. Ph.D. thesis, Universidade Federal do Paraná, Curitiba, PR, Brazil.
- Bird, R. B. and Stewart, W. E. and Lightfoot, E. N., 2002. Transport phenomena. John Wiley & Sons, United States, 2nd edition.
- Falcão Filho, J.B.P., Avelar, A.C. and Reis, M.L.C., 2009. "Historical review and future perspectives for pilot transonic wind tunnel of IAE". *Journal of Aerospace Technology and Management*, Vol. 1, No. 1, pp. 19–27.
- Falcão Filho, J.B.P. and Mello, O.A.F., 2002. "Descrição técnica do Túnel Transônico Piloto do Centro Técnico Aeroespacial". In *Proceedings of the IX Congresso Brasileiro de Engenharia e Ciências Térmicas*. Caxambu, Minas Gerais.
- Liu, T., Sullivan, J.P., 2005. *Pressure and Temperature Sensitive Paints*. Springer, New York.
- McBride, B.J., Gordon, S. and Reno, M.A., 1993. "Coefficients for calculating thermodynamic and transport properties of individual species". NASA Technical Memorandum 4513, NASA.
- Roache, P.J., 2009. *Fundamentals of Verification and Validation*. Hermosa, Albuquerque.
- SAE, 1990. "Aerothermodynamic test instrumentation and measurement". Technical Report AIR 1168/5, Society of Automotive Engineers.
- Sutton, G.P. and Biblarz, O., 2001. *Rocket propulsion elements: an introduction to the engineering of rockets*. John Wiley & Sons, United States, 7th edition.

7. RESPONSIBILITY NOTICE

The authors are the only responsible for the printed material included in this paper.